Journal of the Korean Magnetic Resonance Society **1999**, *3*, 90-99

^{11}B Quadrupole Interaction Studies of Boron-doped Graphite Electrode for Lithium Secondary Battery

Youngil Lee [a,*], Duk-Young Han [b], Donghoon Lee [c], Ae Ja Woo [d], Sam Hyeon Lee [e], Kyung Han Kim [f], and Man Ho Lee [g]

[a] Chemical Analysis Lab, Dongbu Research Council, Taejon, 305-380 Korea
[b] Structural Analysis Division, Korea Basic Science Institute, Seoul, 136-701 Korea
[c] Department of Physics, Pai Chai University, Taejon, 302-735 Korea
[d] Department of Science Education, Ewha Woman's University, Seoul, 120-750 Korea
[e] Department of Physics, Yonsei University, Seoul, 120-749 Korea
[f] NMRi R&D Center, Chi Inc., Yusung-gu, Taejon, 305-340 Korea
[g] Department of Industrial Chemistry, Kyungbuk National University, Taegu, 702-701 Korea
Received August 19, 1999

Abstract: Doping of boron atoms in graphite has been well known method to increase the discharge capacity as the negative electrode material for lithium secondary battery. Herein, the boron-doped graphites are prepared by mixing 1, 2.5, 5, and 7 wt. % of boron carbide in carbon during the graphitizing process. The structural states of boron in boron-doped graphites are investigated by solid-state ^{11}B NMR spectroscopy. The resonance lines for substitutional boron atoms are identified as the second order quadrupolar powder pattern with the quadrupole coupling constant, Q_{CC} = 3.36(2) MHz. The quantitative analysis of ^{11}B NMR spectra with boron-doped graphite has also been performed via simulation.

INTRODUCTION

Doping of boron to carbon matrices is one of well-known methods to improve the discharge capacity of negative graphite electrode for lithium secondary battery. Because the boron atom has fewer electron than carbon, it acts as electron acceptor.[1] While the boron modifies the electronic properties of the graphite without large distortion of the crystal structure, its electron deficiency in carbon matrices creates the 'hole-carrier' in the valence band. Thus, boron-doped graphites have the enhancement of the electrical conductivity, which offer higher discharge capacity. However, the discharge capacity of graphite electrode for lithium storage is relatively limited comparing with lithium metal

used previously.

Since Lowell had introduced the doping of boron atoms into carbon matrices by heating carbon with boron carbide in 1960s,[2] there were many attempts to characterize the states of boron atoms in graphite via X-ray photoelectron spectroscopy (XPS), Raman spectroscopy, and Auger electron spectroscopy, etc.[3-5] But, none of them gave satisfactory results to understand chemical environments of the boron atoms in graphite which are believed to be related with discharge capacity as the electrode of lithium secondary battery. Recently, ^{11}B nuclear magnetic resonance (NMR) spectroscopy had been used to characterize the chemical bonding of boron substituted carbon by Shrasaki *et al.*[6] Even the preliminary results were partially satisfactory for substituted boron atoms which are observed in NMR lines by second-order quadrupole interaction, but unacceptable of the excess boron atoms which reformed to the boron carbide consisting of three boron sites with different quadrupole interactions. Herein, the boron-doped graphites by mixing variable concentrations of boron carbide to carbon were investigated in full detail by ^{11}B NMR spectroscopy along with their corresponding computer simulations.

Boron carbides ($B_{(1-x)}C_x$) exist as a single-phase material over a wide range of carbon concentrations, $0.1 \leq x \leq 0.2$.[7] Boron carbides containing 20 at.% of carbon atoms are composed primarily of $B_{11}C$ icosahedra linked by C-B-C chains. Boron atoms of the boron carbides occupy three major sites: two sites (namely, $6h_1$ and $6h_2$) in each icosahedrons and the other site in a C-B-C chain (1b site). Boron atoms in $6h_1$ (equatorial) site are bonded to carbon atoms in C-B-C chains while boron atoms in $6h_2$ (rhombohedral) site are linked to other boron atoms positioned in the neighboring icosahedra. ^{11}B NMR studies have reported that the quadrupole coupling constants (Q_{CC}) range of the icosahedral sites are from 0.06 to 0.7 MHz for $6h_1$, and from 0.9 to 1.3 MHz for $6h_2$.[8-11] On the other hand, Q_{CC} of boron atoms in the chain site (1b) is reported as 5.58 MHz[8], 5.4 MHz[9], and 5.54 MHz[11] by second-order quadrupole interaction. The conclusion about its structure has not been reached yet. The difficulty is due to an entanglement of strong quadrupole and chemical shift anisotropy interaction for ^{11}B atoms. ^{11}B NMR studies of the boron carbide by authors are underway to determine parameters of quadrupole interaction with its structure having three boron sites.

NUCLEAR QUADRUPOLE INTERACTION

For a nucleus with a spin angular momentum greater than 1/2, such as boron ($I = 3/2$), which has a non-spherical charge distribution, the solid state NMR spectrum is usually dominated by the nuclear quadrupole interaction. A quadrupole nucleus possesses an electric quadrupole moment, eQ, which can interact with the electric field gradient produced by neighboring charges. This interaction is called the nuclear quadrupole interaction; the common form of the Hamiltonian[12] is given by

$$H_Q = \frac{hQ_{CC}}{4I(2I-1)}[3I_z^2 - I^2 + \frac{\eta^2}{2}(I_+^2 + I_-^2)], \qquad [1]$$

where I_z and I^2 are angular momentum operators and I_+ and I_- are the raising and lowering operators for I. The quadrupole coupling constant, Q_{CC}, is defined as

$$Q_{CC} = \frac{eV_{zz}Q}{h} = \frac{e^2q_{zz}Q}{h}, \qquad [2]$$

where e is the electrostatic unit of charge, and Q is the size of nuclear quadrupole moment. The electric field gradient, V_{ij} (= eq_{ij}), can be described by a symmetric 3X3 traceless tensor.[13] The electric field gradient asymmetry parameter, η, is as

$$\eta = \frac{V_{xx} - V_{yy}}{V_{zz}}, (0 \le \eta \le 1) \qquad [3]$$

where the electric field gradient is defined so that $|V_{zz}| > |V_{xx}| > |V_{yy}|$.[14] Here, Q_{CC} represents the strength of the quadrupole interaction, and η describes the departure of the electric field gradient from cylindrical symmetry.

In the presence of a magnetic field, H_Q is treated as a perturbation on the Zeeman Hamiltonian, $H_Z = -\gamma B_o I$. Using first order perturbation theory, the $m \leftrightarrow m$-1 transition appears at the frequency[15]

$$\nu_{m\leftrightarrow m-1} = \nu_o - \nu_Q[\frac{(3\cos^2\theta - 1)}{2} - \frac{1}{2}\eta\sin^2\theta\cos 2\phi](m - \frac{1}{2}), \qquad [4]$$

where ν_o is the Larmor frequency (= $\gamma B_o/2\pi$), m is the magnetic quantum number, and

$$\nu_Q \equiv \frac{3Q_{CC}}{2I(2I-1)}. \qquad [5]$$

The angles θ and ϕ are the Euler angles to the principal axes of the magnetic field. As shown in equation (4), the first order quadrupole interaction is magnetic field independent, such as that of $6h_1$ and $6h_2$ boron sites in boron carbide.

If the quadrupole interaction is large enough to require second order perturbation theory, then the central line is only observed and shifted with the frequency[16]

$$\nu_{\frac{1}{2}\leftrightarrow-\frac{1}{2}} = \nu_0 - (R/6\nu_0)[A(\phi)\cos^4\theta + B(\phi)\cos^2\theta + C(\phi)], \qquad [6]$$

where

$$\begin{aligned} R &= \nu_Q^2[I(I+1) - \tfrac{3}{4}], \\ A(\phi) &= -\tfrac{27}{8} - \tfrac{9}{4}\eta\cos 2\phi - \tfrac{3}{8}\eta^2\cos^2 2\phi, \\ B(\phi) &= -\tfrac{30}{8} - (\eta^2/2) + 2\eta\cos 2\phi + \tfrac{3}{4}\eta^2\cos^2 2\phi, \\ C(\phi) &= -\tfrac{3}{8} + (\eta^2/3) + (\eta/4)\cos 2\phi - \tfrac{3}{8}\eta^2\cos^2 2\phi. \end{aligned} \qquad [7]$$

Notice that the frequency shift from the second order perturbation term is inversely proportional to the Larmor frequency, ν_o. Namely, the second order quadrupole interaction is inversely dependent on the magnetic field, such as that of 1b boron sites in boron carbide.

EXPERIMENTAL

^{11}B NMR experiments were accomplished with boron-doped graphites, which were prepared by carbon mixed with 1, 2.5, 5, and 7 wt.% of boron carbide during the graphitization process. The boron carbide was used as a reference sample to determine the relation between pulse length and tip angle at 64.251MHz using Varian Unity Inova 200 with 4.7 T Oxford magnet. With 10 s of relaxation delay, ^{11}B rf pulse was typically 4.2 μs for a 90° tip angle in 10 mm Chemagnetics' broadband probe. The solid echo pulse sequence ($90°_x$-τ_1-$90°_y$-τ_2-acquisition)[17,18] was chosen to use for boron carbide and boron-doped graphite mixed with 7 wt.% of boron carbide, because broadened NMR lines were dominated by first order quadrupole interaction. Somewhat the second order quadrupole echo pulse sequence ($90°_x$-τ_1-$180°_y$-τ_2-acquisition)[19] was preferred for the boron-doped graphites mixed with 1, 2.5, and 5 wt.% of boron carbide, which NMR lines were ruled by second order quadrupole interaction. The first delay between pulses, τ_1, was 30 μs, and the second delay before echo acquisition, τ_2, was 13 μs. The acquired time domain spectra were Fourier transformed from the top of the echo peak. Because of the ^{11}B quadrupole interaction, all spectra were acquired with quite broad spectral width of 0.5 MHz. To increase the signal-to-noise ratio of the spectra, the signals were averaged from 100 to 6000 times depending on the concentration of boron atoms in the samples. In general, the probe detuning effects from electric conductivity were overcome by mixing the sample with approximately 30 % (v/v) of NaCl filler material.

RESULTS AND DISCUSSION

^{11}B NMR studies have been successfully performed to observe all the boron atomic sites in boron-doped graphites. First of all, static ^{11}B NMR spectrum of the boron carbide has been obtained as shown in Fig. 1(a), which is a combination from several different line broadening mechanism from boron atoms located at three different chemical sites. From previous study, 1b site has very strong quadrupole interaction. Its quadrupole coupling constant is 5.58 MHz with near zero asymmetric parameter, η, based on the second order quadrupolar broadening.[11] Quadrupole coupling constants for $6h_1$ and $6h_2$ sites are relatively weak, so that sideband transition is observed. Baselines rising toward the center in Fig. 1(a) actually turn out to be the sideband transitions. In order to assure the presence of the sidebands, carrier frequency for observation is shifted by 200 kHz, and the same spectrum is obtained.

Spectrum simulation has been performed under the Levenberg-Marquardt nonlinear least-squares algorithm[20,21] which is recorded in Matlab, a vector-oriented programming language, and used in a program to fit an experimental with a simulated spectrum. The quadrupole coupling constants of three boron atomic sites are distinguishably calculated with consideration of isotropic chemical shift. Dipolar broadening is not considered in simulation, since it was minor effect compared to quadrupole and chemical shift anisotropy broadenings. Based on a number of simulations of ^{11}B NMR line shapes for boron carbide, the experimental spectrum can be well simulated with three boron sites. While Q_{CC} value of 1b boron site is 5.58MHz with $\eta = 0$, approximate values of Q_{CC} for two boron sites in icosahedral are obtained by the best fits as judged by χ^2 values and comparison with a set of simulations; 0.51(2) for $6h_1$ and 1.28(4) MHz for $6h_2$ with fixed $\eta = 1$. The extracted quadrupole coupling constants for each boron sites are in the range of previously reported values. Also, isotropic chemical shift tensors are simultaneously extracted for each boron sites; σ_{11} = -176(7), σ_{22} = -91, and σ_{33} = 192 ppm for $6h_1$, σ_{11} = -241(7), σ_{22} = 45, and σ_{33} = 121 ppm for $6h_2$, and σ_{11} = -412(5), σ_{22} = -82(5), and σ_{33} = -44(3) ppm for 1b. The best fitted spectrum is displayed by solid line in Fig. 1(a) with experimental spectrum (pointed line). Fig. 1(b) shows three simulated spectra for different boron sites.

Figure 2(a) shows ^{11}B NMR spectrum of boron-doped graphite mixed with 1 wt.% of boron carbide. The spectrum displays a typical second order quadrupole broadened powder pattern with a small asymmetry parameter, η. Even though the data is not shown, a spectrum with this sample at 7.05 T is obtained, which confirmed that it is the second order quadrupole ^{11}B NMR powder pattern. Also, satisfactory simulated spectrum certifies that the spectrum is broadened by second order quadrupole interaction with Q_{CC} = 3.36(2) MHz and null η. Isotropic chemical shift tensors are obtained as σ_{11} = -48(3), σ_{22} = -33(4), and σ_{33} = -32(3) ppm, respectively. As shown in Fig. 2(a), boron-doped graphite mixed with 1 wt.% of boron carbide has a boron atomic site having identical Q_{CC} and chemical

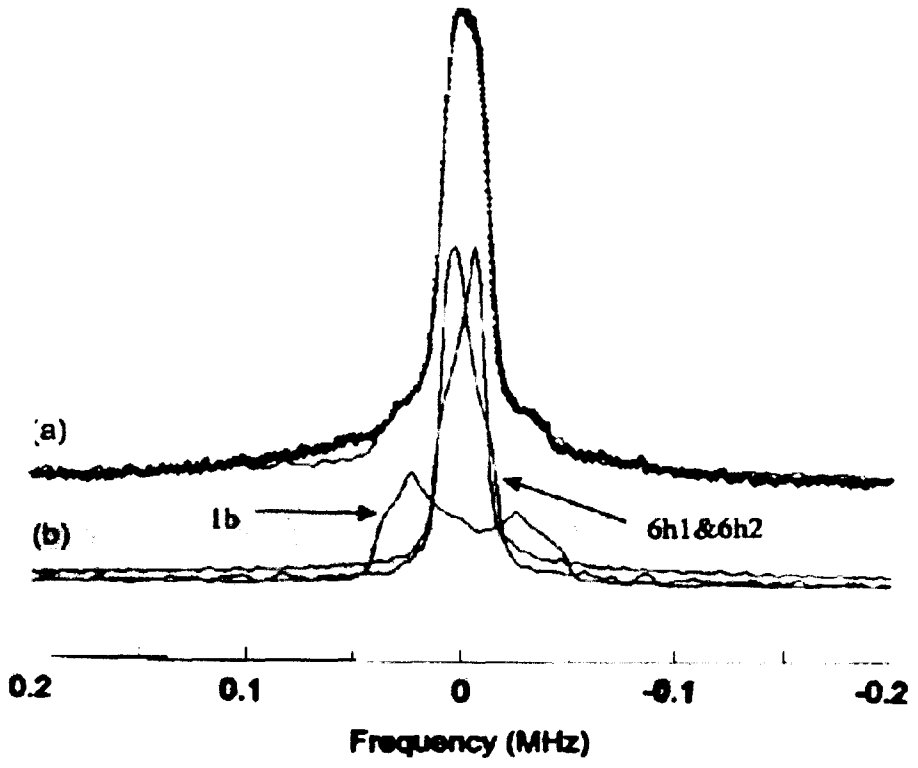

Fig. 1. (a) The ^{11}B NMR spectra of the boron carbide with experimental (displayed by points) and simulated (solid line) data. (b) The simulated spectra of each ^{11}B sites; Q_{cc} = 0.51(2) and 1.28(4) MHz for $6h_1$ and $6h_2$ boron sites with fixed $\eta = 1$, and $Q_{cc} = 5.58$ MHz for 1b boron site with $\eta = 0$.

shift tensors, which are not the same as those of boron carbide. It indicates no trace of the boron carbide in graphite mixed with 1 wt.% boron carbide, so that these boron atoms in graphite can be only located in the substitutional site replacing carbon atoms. Furthermore, null value of η indicates the boron atomic sites are in the hexagonal planar symmetry which graphite should have.

With excellent simulated NMR data as clarified above, ^{11}B NMR spectra of boron-doped graphites mixed with 2.5, 5, and 7 wt.% of boron carbide are successively analyzed as shown in Figs. 2(b)-(d). Based on a number of simulations of ^{11}B NMR line shapes for boron-doped graphites, the experimental spectra cannot be simulated with a single boron site as for the case of boron-doped graphite mixed with 1 wt.% of boron carbide. Also, there are distinctive features in the spectra that indicate three boron sites from boron carbide. Thus, experimental and simulated ^{11}B NMR spectra as shown in the figures contain not only

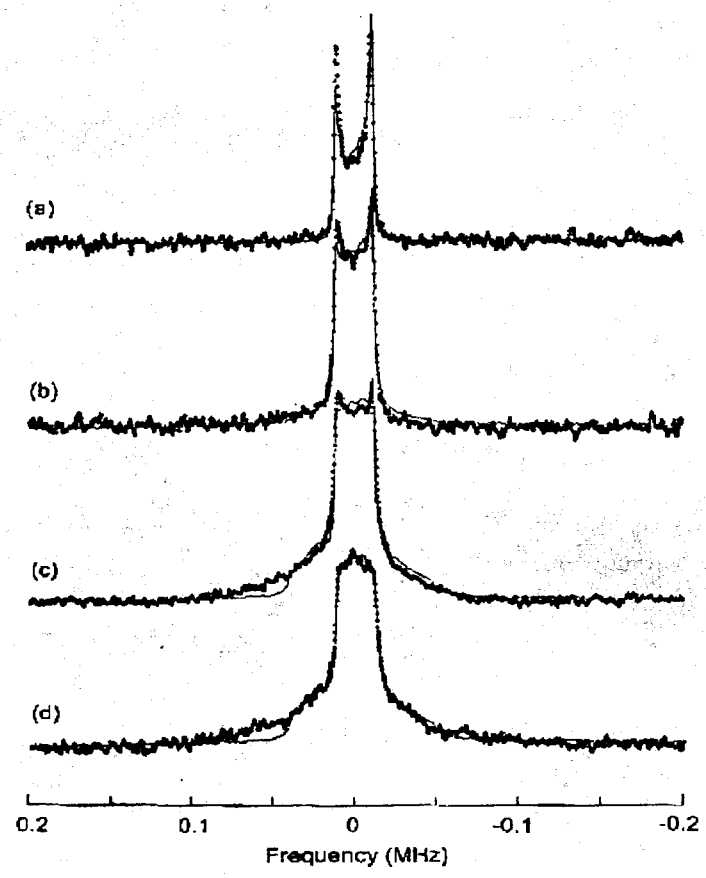

Fig. 2. The ^{11}B NMR spectra of the boron-doped graphite mixed with (a) 1, (b) 2.5, (c) 5, and (d) 7 wt.% of boron carbide with experimental (displayed by points) and simulated (solid line) data.

the ^{11}B peak of substitutional site in graphite as same as in boron-doped graphite mixed with 1 wt.% of boron carbide, but also ^{11}B peaks of three sites in boron carbide itself. The observation of ^{11}B NMR peaks for boron sites of boron carbide proves the saturation of the substitutional site in boron-doped graphites, due to the solid solubility limit of boron in graphite. Thus, it is expected that the excess boron atoms in boron-doped graphite are restructuring to the boron carbide inside graphite.

Meanwhile, the ^{11}B peak of the substitutional site in graphite has not changed much, the portion of ^{11}B peaks of three sites from boron carbide is exponential-growthly increased depending on the concentration of boron carbide mixed in carbon graphitizing process. Simulation results of ^{11}B NMR spectra for boron-doped graphites are fairly satisfactory.

Table 1 shows the relative integral ratio of each boron sites for the concentration of boron carbide mixed in graphites via the simulation of spectra. For boron-doped graphite mixed with 1 wt.% of boron carbide, the boron sites from boron carbide has not been considered. Following ^{11}B NMR results, all boron atoms in graphite substitute carbon atoms in low concentration, such as 1 wt.%, of boron carbide mixture, and locate at the trigonal sites in the graphite lattice which is structured by graphite planes. However, excessive boron atoms in graphite are subject to diffuse along planar channels provided by graphite planes in high concentration of boron carbide mixture. Since boron atom is known as a fast diffusant because of its light mass, it is free to find a stable site. The possible site would be grain boundary where enough space is available and free for boron atoms to reform their own structure, which is the boron carbide. This formation of the boron carbide around grain boundary region certainly acts as a hindrance to free migration of charge carrier. It can be explained that the discharge capacity of the boron-doped graphite as negative electrode is genuinely correlated with the contents of substitutional boron atoms. However, excessive additions of boron atoms into graphite above its solid solubility limit will choke entrances of charge carriers to graphite planes.

Table 1. The relative quantity ratio of each boron sites for the concentration of boron carbide mixed in graphites via computer simulation. A value in each parenthesis denotes a standard deviation of the corresponding data value.

Boron-doped graphite	^{11}B site			
	Substitutional	$6h_1$	$6h_2$	1b
1 wt.% boron carbide	1	0	0	0
2.5 wt.% boron carbide	1	0.78(9)	0.78(9)	0.05(1)
5 wt.% boron carbide	1	1.2(1)	1.2(1)	0.40(2)
7 wt.% boron carbide	1	2.4(3)	2.4(3)	0.71(7)

CONCLUSION

The ^{11}B NMR spectra for substitutional site in boron-doped graphites had been successfully observed at 4.7 T and analyzed via complete simulation. The maximum solid solubility of boron atoms to graphite could be in between 1 and 2.5 wt.% of boron carbide mixed graphite. As more boron atoms were mixed in graphite, the excessive boron atoms obviously are suspected to recrystallize into the boron carbide. Grain boundary of graphite could be the probable place for it, since boron atoms can be reformed to the most stable configurations among themselves, which is the boron carbide. In this work, we were able to fit to ^{11}B NMR spectra for boron-doped graphites by combining ^{11}B NMR spectrum of the boron carbide and substitutional boron in 1 wt.% of boron carbide mixed graphite. The quantitative analysis of ^{11}B NMR spectra with boron-doped graphite had also been performed via simulation. Experimental results had proper agreement, which were adequate to understand the function and the structural states of boron atoms in boron-doped graphites.

REFERENCES

1. A. Marchand, *Chem. Phys. Carbon*, **7**, 155 (1971).
2. C.E. Lowell, *J. Am. Ceram. Soc.*, **50**, 142 (1967).
3. M. Koh and T. Nakajima, *Electrochimica Acta*, **44**, 1713 (1999).
4. R. Jimbou, M. Saidoh, K. Nakamura, M. Akiba, S. Suzuki, Y. Gotoh, Y. Suzuki, A. Chiba, T. Yamaki, M. Nakagawa, K. Morita, and B. Tsuchiya, *J. Nucl. Mater.*, **233-7**, 781 (1996).
5. B. Ottaviani, A. Derré, E. Grivei, O.A.M. Mahmoud, M. Guimon, S. Flandrois, and P. Delhaès, *J. Mater. Chem.*, **8**, 197 (1998).
6. B. Ottaviani, A. Derré, E. Grivei, O.A.M. Mahmoud, M. Guimon, S. Flandrois, and P. Delhaès, *J. Mater. Chem.*, **8**, 197 (1998).
7. D. Emin, G. A. Samara, and et al., *J. Less-Common Met.*, **117**, 415 (1986).
8. A. H. Silver and P. J. Bray, *J Chem. Phys.*, **31**, 247 (1959).
9. T. V. Hynes and M. N. Alexander, *J. Chem. Phys.*, **54**, 5296 (1971).
10. T. V. Hynes and M. N. Alexander, *J. Chem. Phys. Erratum*, **56**, 681 (1972).
11. D. Lee, P. J. Bray and T. L. Aselage, *J. Phys.: Condens. Matter.*, **11**, 4435 (1999).
12. E.A.C. Luken, "Nuclear Quadrupole Coupling Constants", Academic Press, New York, 1969.
13. C.P. Poole and H.A. Farach, "Theory of Magnetic Resonance", Wiely-Interscience, New York, 1987.
14. Y.A. Buslaev, E.A. Kravcenko, and L. Kolditz, *Coord. Chem. Rev.*, **82**, 1 (1987).
15. M.H. Cohen and F. Reif, "Solid State Physics Vol. 5", Academic Press, New York, 1957.

16. K. Narita, J. Umeda, and H. Kusumoto, *J. Chem. Phys.*, **44**, 2719 (1966).
17. P. Mansfield, *Phys. Rev.*, **137**, 961 (1965).
18. W.W. Jr. Warren and R.E. Norberg, *Phys. Rev.*, **154**, 277 (1967).
19. D. Han and H. Kessemeier, *Phys. Rev. Lett.*, **67**, 346 (1991).
20. W. H. Press, B. P. Flannery, S. A. Teukolsky, and W. T. Vetterling, "Numerical Recipes", Cambridge University Press, Cambridge, 1986.
21. A. J. Kim and L. G. Butler, *Concepts in Magnetic Resonance*, **4**, 205 (1992).